Electronic Supplementary Material (ESI) for Nanoscale Horizons.

Electronic Supplementary Information

Atomic-Scale Dents on Cellulose Nanofibers: the Origin of Diverse Defects in Sustainable Fibrillar Materials

T. Ito, K. Daicho, S. Fujisawa, T. Saito, and K. Kobayashi**

This file includes Experimental methods, Figures S1−S6, and Table S1.

Experimental methods

Sample preparation. Four CNFs dispersions (DC, US, HP4, HP50) were prepared from a TEMPO-oxidized pulp (DKS Co. Ltd., Kyoto, Japan, carboxylate content of 1.8 mmol/g) by wet disintegration using three different homogenizers. For preparing the dispersion DC, the 0.2% pulp suspension was treated with a double-cylinder homogenizer (Physcotron NS-56, MICROTEC Co., Ltd.), equipped with a 20 mm shaft, at 7500 rpm for 80 min. To prepare US, the 0.1% pulp suspension was pretreated with a double-cylinder type homogenizer for 5 min and was subsequently sonicated using an 18 mm probe (US-300E, NISSEI Corporation) at an output power of 80% for 5 min. For the preparation of the dispersions HP, 1 L of the 0.5% pulp suspension was passed (4 times for HP4 and 50 times for HP50) through a high-pressure homogenizer (HJP-25001, Sugino Machine) at 150 MPa. All samples were passed through a 20 μm mesh filter once to remove unfibrillated fractions.

Atomic force microscopy (AFM). CNF dispersions were diluted to 0.0002% (w/w) with distilled water and dropped onto freshly cleaved mica surfaces. This was followed by drying for 15 min under vacuum conditions. AFM observations were performed using a MultiMode 8 microscope (Bruker, USA) equipped with a NanoScope V controller and ScanAsyst-Air (tip radius of 2 nm) in PeakForce Tapping mode. The sensitivity of the photodetector was calibrated for every measurement, and the spring constants of all the cantilevers were calculated. The peak force applied to the CNFs during the measurement was set to 2.000 nN. The images were acquired with a scanning area of 2 × 2 μm^2 and 1024 × 1024 pixels.

Calibration of the AFM images. Background calibration process was applied to every 1024 rows of the AFM images. The curved background of the AFM images was flattened by this calibration (Figure S2). The outlier heights of each row were excluded in order to extract the curved background. First quartile (Q_1), third quartile (Q_3) and interquartile range (IQR) of heights in each row were used to calculate thresholds. Upper and lower outlier thresholds were set at Q_1 – 1.5 * IQR and Q_3. The curved background was fitted with Savitzky-Golay filter (window size = 31, degree of polynomial = 2). This fitting curve was subtracted from the initial height profile so that the background height was set at 0 nm. Finally, median filter with kernel size of 3×3 pixels was applied to remove noise.

Image processing. We analyzed the AFM images using image processing as shown in Figure S1. We extracted the centerline of the CNFs, from which we evaluated the heights of the CNFs and detected the kinks and end points. The programs were all implemented in Python 3.8.1 using NumPy (1.21.2),[1] OpenCV (4.5.4.60),[2] scikit-image (0.18.3),[3] SciPy (1.7.1),[4] and mahotas (1.4.12).[5]

Background calibration and noise reduction were applied to all the AFM images (Figure S2). First, binarization was performed to extract CNFs regions from the AFM images. We used global binarization with a threshold of 0.3 nm and adaptive binarization with a window size of 17 pixels. A Gaussian filter was used to determine the threshold value for adaptive binarization. The regions extracted by both global and adaptive binarization were determined to be the CNFs regions. To distinguish each CNF region, each region was labeled individually. Subsequently, we removed the small fractions that satisfied all the three conditions: (1) the percentage of linear components calculated from the probabilistic Hough transformation[6] was less than or equal to 30%; (2) the maximum height within each CNF region was less than 1.5 nm; (3) the number of pixels in each CNF region was less than 200. We also extracted the approximate centerline of the CNFs region using a thinning algorithm.[7] The centerline contains short branch-like artifacts after thinning; therefore, these branches were removed to determine the final centerline of the CNFs (Figure S3). We determined the positions of the kinks on the CNFs based on the shape of the centerlines. We calculated the approximate straight lines around the pixel of interest on the centerline. When the angle between the approximate straight lines was greater than or equal to 30°, the pixel of interest was assigned as a kink. The kinks thus detected are shown with the end points in Figure S1. We obtained the height profiles of the CNFs after converting the pixel distance to nanometers.

AFM simulation. The AFM tip was assumed to be a sphere with a radius of 2 nm, and the lower limit of the tip when it collided with the CNF was calculated (Figure S4). We considered the case when the cross-section of a CNF was in the scan direction, and the CNF was stably adsorbed on the substrate. With a constant tap interval (2 nm in this study), the height profile of the cross-section was determined based on the relative position of the tapping point and the CNF. The calculation was repeated while shifting the tap position by 2 nm with a step size of 0.1 nm; this provided all possible patterns of the height profile for a given cross-sectional model. As we

extracted the centerlines of the CNFs from the AFM images, the height at the center of the obtained profile corresponds to the measured height. If the height profile had an even length, the average height of the two centers was adopted. The height profiles shown in Figure S4b correspond to the cases that provide the maximum and minimum heights of the CNF. The range between these heights was determined as the possible range of CNF observed by AFM measurements.

The indentation of the tip was ignored in this simulation for the following reason. The Hertzian model, which refers to the contact of a sphere and an elastic half-space, is described as

$$F = \frac{4}{3}\frac{E}{1-\nu^2}\sqrt{R}\delta^{3/2}$$

where F is the applied force, ν is the Poisson's ratio, δ is the indentation, and R is the radius of the indenter (tip radius). F and R were set to 2.000 nN and 2.0 nm, respectively. The values of Poisson's ratio ([200]/[004] = 0.377, [110]/[004] = 0.639, and [1-10]/[004] = 0.442) and Young's modulus (= 30 GPa) used in this calculation are those reported in previous studies.[8, 9] According to the calculation based on the Hertzian model, under the conditions in this study, the maximum nanoindentation was approximately 0.1 nm. This nanoindentation was sufficiently small compared with the noise (std = 0.19 nm).

Table S1. Total length, the number of AFM image, and the number of CNF observed for each sample.

	Total length (nm)	**Number of AFM image**	**Number of CNF**
DC	50516	9	39
US	110004	10	203
HP4	79695	11	156
HP50	156857	14	416

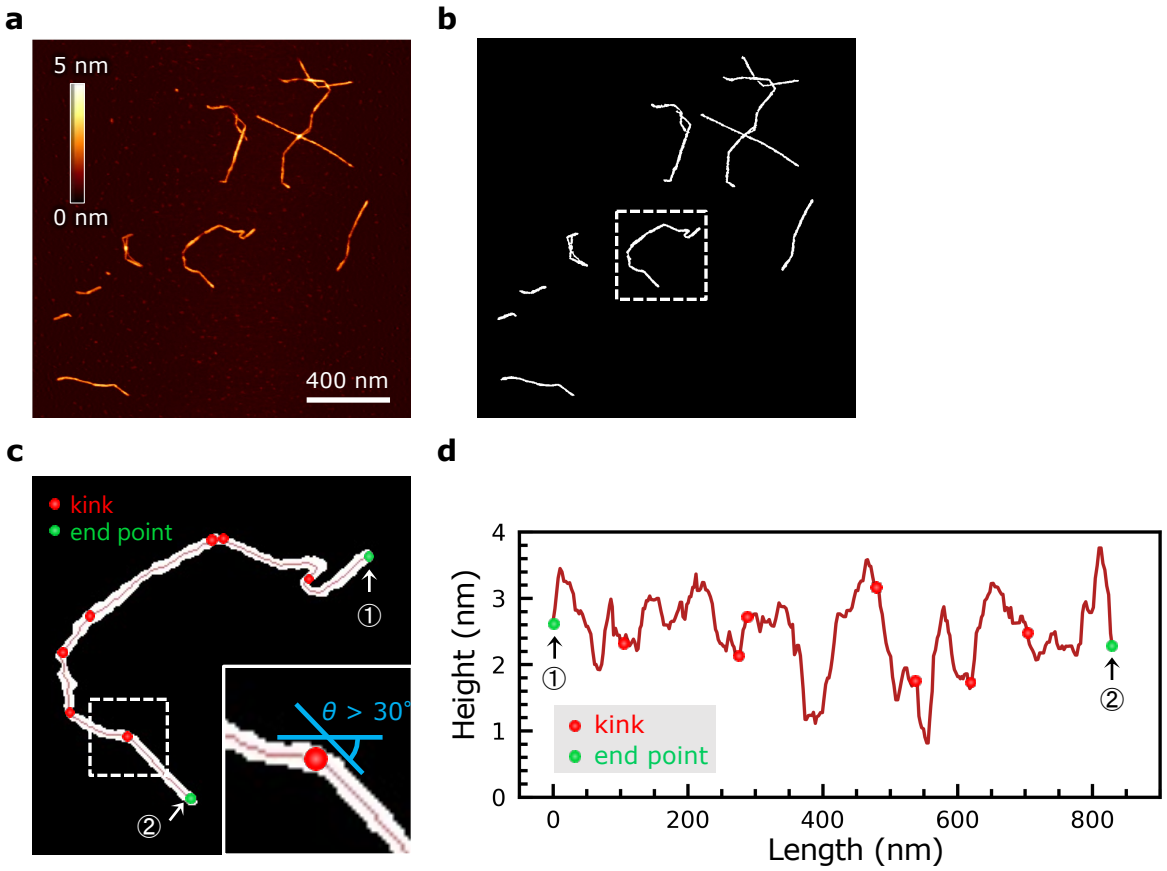

Figure S1. Image processing extracts geometric information of CNFs from the AFM images. (a) AFM image of HP4 after background calibration. (b) Binarization is applied to the AFM images. The CNFs regions (white) are separated from the background (black). (c) Thinning algorithm transforms a binarized region (white) to a 1-pixel centerline (red line). The image is the magnified region from (b). The red and green dots represent kinks and end points detected along the centerline. (c, inset) Kinks were detected when their angles were over 30°. The image is the magnified region from (c). (d) Height profile along the centerline of the CNF shown in (c) with the corresponding kinks (red dots) and end points (green dots). The end points numbering 1, 2 correspond to those in (c).

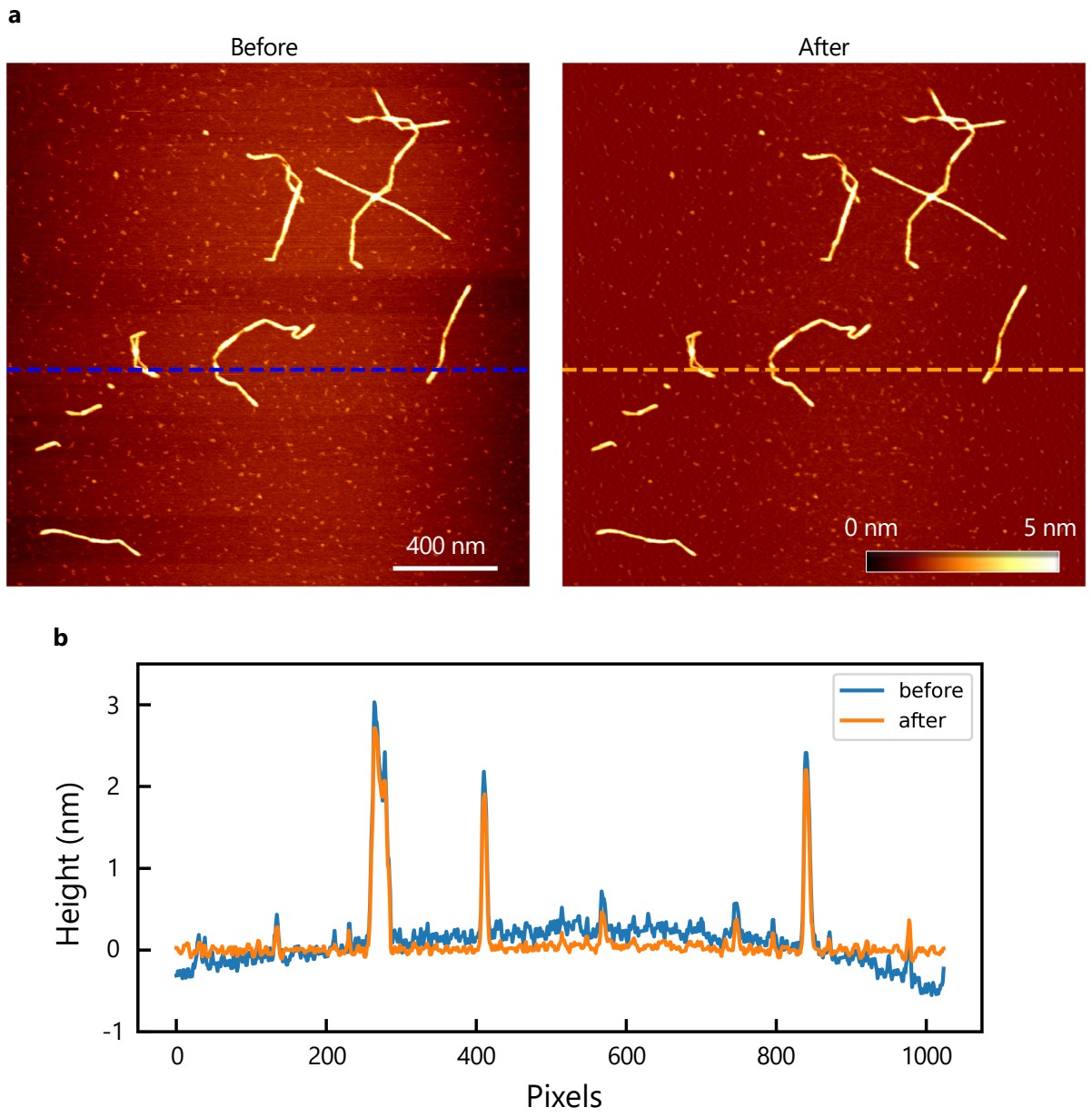

Figure S2. (a) AFM images of HP4 before the background calibration (left) and after the calibration (right). (b) Height profile along the blue and orange lines in (a).

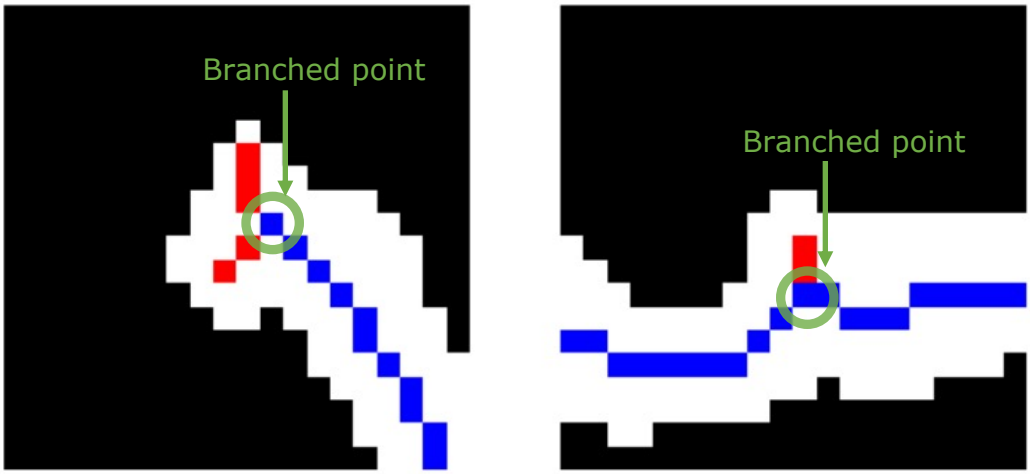

Figure S3. Typical images of branch like red lines at the end of CNFs (left) and in the middle of blue centerlines (right) due to the rough contour of binarized image. These branches are removed based on two criteria: (1) the height at each branched point (indicated with green circle) is equal to or lower than 5 nm, (2) the length of each branch is shorter than 9 pixels. When a branch satisfies these two criteria simultaneously, that branch is removed.

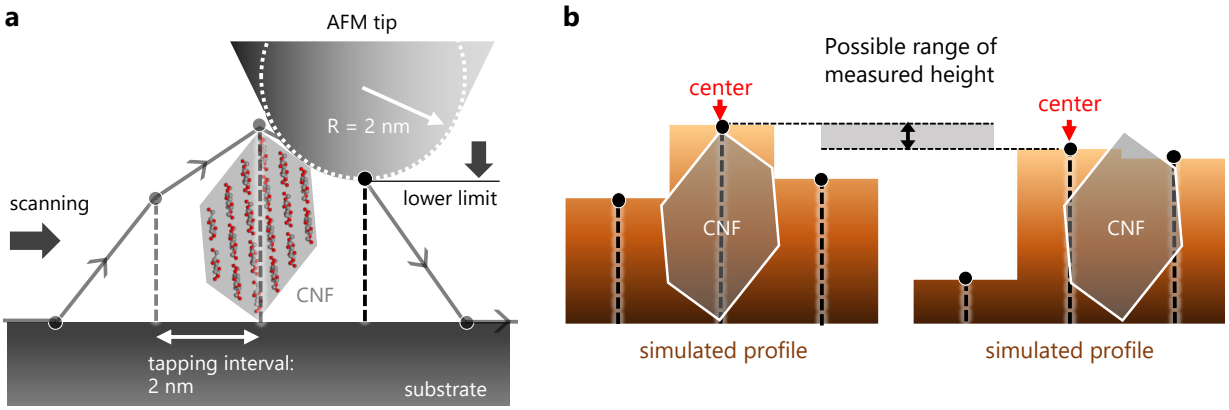

Figure S4. Simulation determines possible range of height obtained by AFM analysis. (a) Situation of AFM measurement. Black dots show points where lower limit of AFM tip reaches when it collides with a CNF. Its distance from substrate (dashed line) corresponds to measured height at tapping point. (b) Pattern of height profile vary depending on relative position of tapping point and CNF. Heights at center of profiles (red arrows) corresponds to calculated height obtained from centerlines of CNFs in AFM images. Two profiles exhibit the cases where maximum (left) and minimum (right) height are recorded, respectively, for the given CNF model. The possible height range obtained by AFM analysis is calculated as the difference between the maximum and minimum heights.

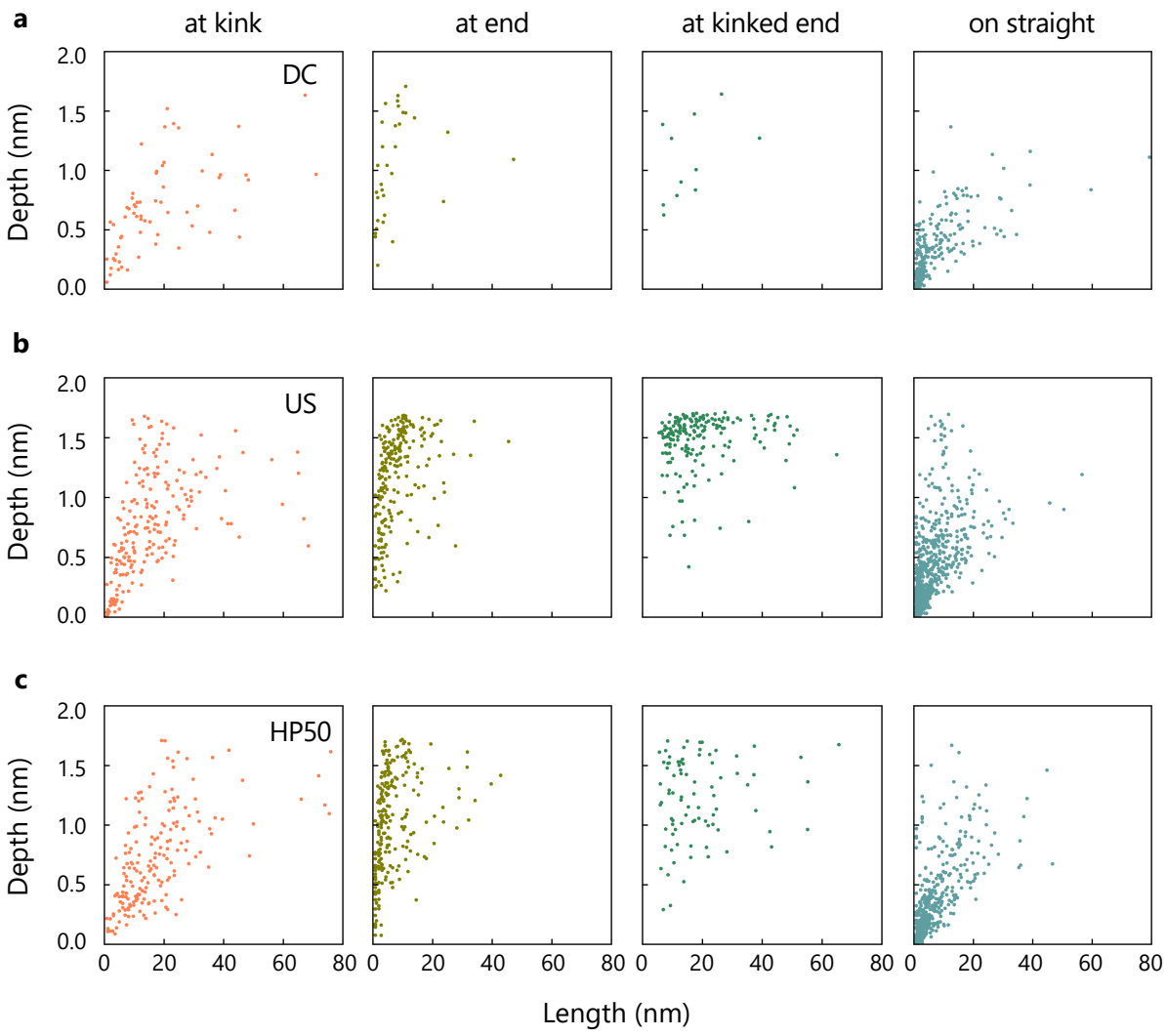

Figure S5. Relationship between the length and the depth of dent defects (‘at kink’, at end’, ‘at kinked end’, ‘on straight’, from left to right). (a) DC, (b) US, (c) HP50.

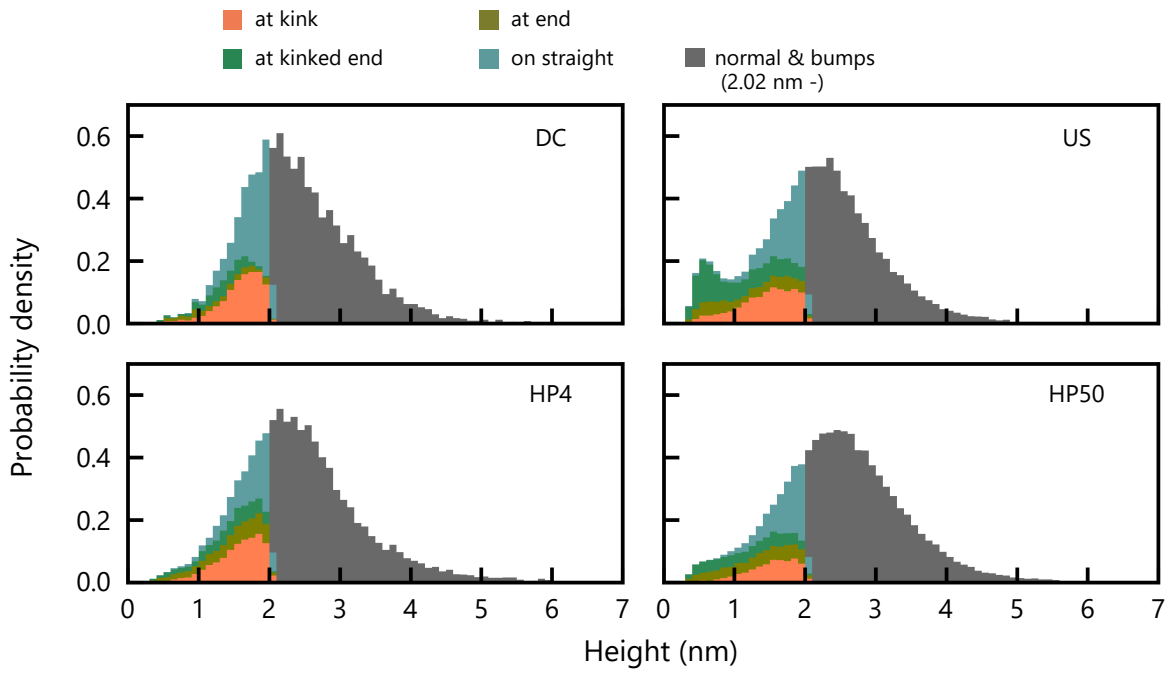

Figure S6. Height distributions with the classification of dent defects.

References

(1) Harris, C. R.; Millman, K. J.; van der Walt, S. J.; Gommers, R.; Virtanen, P.; Cournapeau, D.; Wieser, E.; Taylor, J.; Berg, S.; Smith, N. J.; Kern, R.; Picus, M.; Hoyer, S.; van Kerkwijk, M. H.; Brett, M.; Haldane, A.; Del Río, J. F.; Wiebe, M.; Peterson, P.; Gérard-Marchant, P.; Sheppard, K.; Reddy, T.; Weckesser, W.; Abbasi, H.; Gohlke, C.; Oliphant, T. E. Array Programming with NumPy. *Nature* **2020**, *585*, 357–362.

(2) Bradski, G. The OpenCV Library. *Dr. Dobb's Journal: Software Tools for the Professional* **2000**.

(3) van der Walt, S.; Schönberger, J. L.; Nunez-Iglesias, J.; Boulogne, F.; Warner, J. D.; Yager, N.; Gouillart, E.; Yu, T. Scikit-Image: Image Processing in Python. *PeerJ* **2014**, *2*, e453.

(4) Virtanen, P.; Gommers, R.; Oliphant, T. E.; Haberland, M.; Reddy, T.; Cournapeau, D.; Burovski, E.; Peterson, P.; Weckesser, W.; Bright, J.; van der Walt, S. J.; Brett, M.; Wilson, J.; Millman, K. J.; Mayorov, N.; Nelson, A. R. J.; Jones, E.; Kern, R.; Larson, E.; Carey, C. J.; Polat, İ.; Feng, Y.; Moore, E. W.; VanderPlas, J.; Laxalde, D.; Perktold, J.; Cimrman, R.; Henriksen, I.; Quintero, E. A.; Harris, C. R.; Archibald, A. M.; Ribeiro, A. H.; Pedregosa, F.; van Mulbregt, P.; SciPy 1.0 Contributors. SciPy 1.0: Fundamental Algorithms for Scientific Computing in Python. *Nat. Methods* **2020**, *17*, 261–272.

(5) Coelho, L. P. *Mahotas: Computer Vision in Python*; Github.

(6) Duda, R. O.; Hart, P. E. Use of the Hough Transformation to Detect Lines and Curves in Pictures. *Commun. ACM* **1972**, *15*, 11–15.

(7) Guo, Z.; Hall, R. W. Parallel Thinning with Two-Subiteration Algorithms. *Commun. ACM* **1989**, *32*, 359–373.

(8) Nakamura, K.; Wada, M.; Kuga, S.; Okano, T. Poisson's Ratio of Cellulose Iα and Cellulose II. *J. Polym. Sci. B Polym. Phys.* **2004**, *42*, 1206–1211.

(9) Tanpichai, S.; Quero, F.; Nogi, M.; Yano, H.; Young, R. J.; Lindström, T.; Sampson, W. W.; Eichhorn, S. J. Effective Young's Modulus of Bacterial and Microfibrillated Cellulose Fibrils in Fibrous Networks. *Biomacromolecules* **2012**, *13*, 1340–1349.